THE JOURNAL OF PHYSICAL CHEMISTRY A
A JOURNAL OF THE AMERICAN CHEMICAL SOCIETY

pubs.acs.org/JPCA

Article

Electronic Structures of Small Stoichiometric Zn_xO_x Clusters

Published as part of The Journal of Physical Chemistry A virtual special issue "Richard J. Saykally Festschrift".

Shivangi Vaish, Abigail O. Gyamfi, Caleb D. Huizenga, Hrant P. Hratchian, and Caroline Chick Jarrold*

Cite This: *J. Phys. Chem. A* 2024, 128, 6450−6461

Read Online

ACCESS | Metrics & More | Article Recommendations | Supporting Information

ABSTRACT: Stoichiometric Zn_xO_x clusters in the subnanometer size regime have been the topic of several computational and mass spectrometry studies that showed the particular stability of the stoichiometric species relative to nonstoichiometric species (Zn_xO_y, $x \neq y$). In the current study, we present the angle-resolved anion photoelectron (PE) spectra of stoichiometric $Zn_xO_x^-$clusters ($2 \leq x \leq 5$), which are interpreted with supporting computational studies that include natural orbital ionization calculations on detachment transition cross sections. All spectra show evidence of D_{xh} ring structures, which had been predicted to be the most stable structures in previous computational studies. However, a new lowest energy isomer is reported for the Zn_2O_2 anion and neutral, a bent chain, which is readily reconciled with the most intense feature in the $Zn_2O_2^-$ PE spectrum. The computed PE angular distributions (PADs) associated with the lowest energy cluster structures identified computationally agree with the experimental results, with the exception of $Zn_5O_5^-$, the experimental PAD of which suggests that strong vibronic coupling may be introducing anomalies. While the lowest lying electronic state of the Zn_2O_2 chain structure is a triplet state, all neutral ring structures (including Zn_2O_2, the anion of which also populates the ion beam), favor a singlet electronic state. The computed singlet−triplet splitting of the D_{xh} structures increases monotonically with x. Overall, we find that the properties of the ring structures evolve smoothly, rather than in the punctuated manner typically seen in the small cluster size regime.

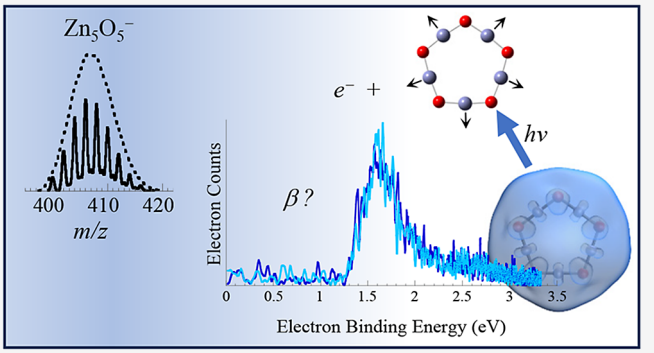

1. INTRODUCTION

The electronic and molecular structures of small transition metal oxide (TMO) clusters have been of enduring interest. Generally, the small cluster size regime is distinguished by species having too few atoms to support a molecular structure that resembles the bulk crystal structure, or for which a bulk-like molecular structure is energetically unfavorable. In this size regime, the cluster properties typically change in a punctuated manner with incremental changes in the number of constituent metal oxide units.[1] At some system-specific size (typically in the nanoscale regime), the bulk structure becomes energetically favored, and cluster properties evolve smoothly toward bulk properties with incremental size increases in a way that is governed by quantum confinement effects.[2,3] This crossover from molecular to bulk-like properties is of technological interest, given the use of TMOs in a wide range of electronics applications.[4,5]

In this report, we present the results of a combined experimental and computational study on small stoichiometric zinc oxide clusters, Zn_xO_x, which follow a different type of evolution of properties with x, in that the small cluster size regime exhibits a smooth evolution of properties with cluster size (x), but with molecular structures that in no way resemble the bulk.

Interest in zinc oxide clusters has propelled several theoretical and experimental studies. Aside from being an inexpensive and nontoxic material, ZnO is a wide bandgap semiconductor that offers promise as a spintronic material when doped with certain TM ions.[6] ZnO has also been investigated as a transparent conductive electrode, an inexpensive alternative to indium tin oxide.[7,8]

The structures of neutral stoichiometric Zn_xO_x clusters were predicted computationally to evolve from ring structures to cage structures somewhere in the x = 6 to 8 range, depending on the computational approach.[9,10] Intermediate-sized clusters form hollow cages,[11] with larger clusters assuming nonhollow 3-dimensional structures.[12−14]

Received: May 31, 2024
Revised: July 8, 2024
Accepted: July 9, 2024
Published: July 31, 2024

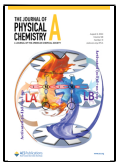

https://doi.org/10.1021/acs.jpca.4c03613
J. Phys. Chem. A 2024, 128, 6450−6461

Experimentally, Gunaratne et al. reported the mass spectrum of small zinc oxide clusters generated using laser ablation, with results suggesting that the stoichiometric clusters are more stable than nonstoichiometric clusters based on relative abundances.[15] They also reported photoelectron (PE) images of $Zn_3O_3^-$ and $Zn_3O_4^-$ that were consistent with calculated ring structures. Time-resolved PE spectra of $Zn_xO_x^-$ (x = 5,8,12−14, 16) reported by Heinzelmann et al.[16] probed the lifetimes of excited doublet states of the anions. They found long lifetimes of excited states that appeared independent of cluster size, at odds with the punctuated changes in cluster properties typically observed in the small cluster size regime, as noted above. In addition, their conventional anion PE spectra of the clusters with $x > 5$ were remarkably similar and showed a gradual (nonpunctuated) increase in neutral electron affinity (EA). This result is puzzlingly evocative of the bulk-like but quantum-confined size regime, as a gradual increase in EA is consistent with the excess electron in the anion being more stabilized with increasing size because of delocalization of the excess charge.

Past studies on TMO clusters from our own group have largely focused on suboxide species,[17−21] which have complex electronic structures associated with unpaired electrons occupying nearly degenerate metal-localized orbitals. Here, we report the angle-resolved PE spectra of small stoichiometric $Zn_xO_x^-$ ($2 \le x \le 5$) clusters along with new theoretical results on the structures and low-lying excited states, and computed photoelectron angular distributions (PADs). This study bridges the gap between studies on the ZnO^- diatomic molecular anion[22−24] and the PE spectra reported by Heinzelmann et al.[16] and provides new insights into the nature of the detachment transition. We tie the appearances of the small cluster spectra to the larger cluster series and identify a more stable structure of $Zn_2O_2^-$ and Zn_2O_2 not reported previously. Our findings suggest that in this small size regime for $x > 2$, the molecular structures evolve smoothly, the singly occupied molecular orbital of the anions can be described as the in-phase combination of x Zn-local 4s orbitals arranged in a ring structure, the spectra are indeed similar in appearance, and evolve smoothly with x, but not toward a bulk-like structure.

2. METHODS

2.1. Experimental Details. Anionic zinc oxide clusters were generated and probed using anion PE spectroscopy using an apparatus that has been described in detail previously.[25−27] Briefly, a broad distribution of $Zn_xO_y^-$ sizes and oxidation states were generated in a pulsed laser ablation/molecular beam valve cluster source. The second harmonic output of a Nd:YAG laser (532 nm, 2.33 eV) operating at 30 Hz with approximately 9 mJ/pulse was focused onto the surface of a rotating pressed Zn powder target (natural abundance isotopic distribution, Alfa Aesar 99.9%). The resulting plume was swept by a pulse of ultrahigh purity helium from a solenoid-type pulsed molecular beam valve through a 25 mm long, 3 mm diameter clustering channel. The gas mixture then expanded into vacuum and passed through a 3 mm skimmer, whereupon the anions were accelerated into a 1.2-m time-of-flight mass spectrometer. After passing through a mass defining slit, the ions entered a detector region and continued to drift until colliding with a dual microchannel plate (MCP) detector. A digitizing oscilloscope was used to record the output of the detector to measure the mass distribution.

While drifting to the ion detector, the anions passed through a laser interaction region at the intersection of the ion drift path and a 1-m field-free photoelectron drift tube situated perpendicular to the ion beam axis. A second Nd:YAG laser was timed to intersect the mass-separated anions, and the small fraction (10^{-4}) of the resulting photoelectrons that traveled the length of a 1-m field-free drift tube orthogonal to the ion drift tube were detected on a second microchannel plate detector. The drift times of the photoelectrons were recorded and converted to electron kinetic energy, e^-KE, calibrating with well-known spectra of O^- and OH^-. The e^-KE was then converted to the photon-independent electron binding energy, e^-BE, which equals the difference in energy between the final neutral states relative and the initial anion state per eq 1

$$e^-BE = h\nu - e^-KE = EA_0 + E_{int}^{neutral} - E_{int}^{anion} \quad (1)$$

where EA_0 is the adiabatic neutral electron affinity, $E_{int}^{neutral}$ is the internal energy (electronic, vibrational, rotational) of the final neutral state, and E_{int}^{anion} is the internal energy of the anion. If the anion is internally cold, the e^-BE distribution reflects the vibronic states of the neutral accessed via photodetachment. In practice, the anions are not fully cooled in the ablation source, and the internal temperatures are estimated to be between 300 and 500 K based on spectral simulations.

All spectra shown below were obtained using 3.495 eV photon energy. In past studies, spectra were collected with several photon energies. However, because of the broad distribution of isotopologues for $(ZnO)_x^-$ species with $x > 2$, spectra had to be collected for over one million shots to achieve reasonable signal-to-noise ratios. Spectra were additionally obtained with the electric field vector of the linearly polarized detachment laser both parallel ($\theta = 0°$) to and perpendicular ($\theta = 90°$) to the electron drift path to determine the PAD. Based on the seminal work of Cooper and Zare,[28] the PADs in terms of photoelectron intensity, I as a function of θ can be described as

$$I_\theta \propto [1 + \beta P_2(\cos\theta)] \quad (2)$$

where P_2 (cos θ) is the second Legendre polynomial, and β is an asymmetry parameter that can assume values between −1 (perpendicular PAD) and 2 (parallel PAD). Isotropic PADs have $\beta = 0$. The asymmetry parameter is calculated from the measured I_0 and I_{90} by

$$\beta = \frac{I_0 - I_{90}}{\frac{1}{2}I_0 + I_{90}} \quad (3)$$

The asymmetry parameter can be related to symmetry of the orbital from which the photoelectron was detached, as extended upon cogently by Sanov.[29]

The spectrum collected for each cluster required over 2 million laser shots including both polarizations. We therefore confined this study to one photon energy.

The e^-KE-dependent line width of atomic transitions (in eq 4) measured by the apparatus is given by[27]

$$\Delta(e^-KE) = 0.004\ eV + 0.0078\ eV \cdot \left(\frac{e^-KE}{eV}\right)^{3/2} \quad (4)$$

Individual rovibronic transitions in molecular species are therefore not resolved. Rotational manifolds broaden transitions for molecular anions. However, some vibrational structure is partially resolved in the spectra presented below.

https://doi.org/10.1021/acs.jpca.4c03613
J. Phys. Chem. A 2024, 128, 6450−6461

2.2. Computational Details. Calculations on previously reported neutral structures along with several alternative neutral structures, and different possible structures of the associated anions were carried out using the GAUSSIAN suite of electronic structure programs, including a local development version.[30,31] The B3LYP/SDDPlusTZ model chemistry has been employed throughout.[32,33] The SDDPlusTZ, which has been used successfully by our groups in prior work,[34−38] includes a Stuttgart/Dresden (SDD) relativistic pseudopotential on the Zn center to treat core electrons, an augmented SDD for metal valence orbitals, and the Dunning correlation-consistent aug-cc-PVTZ[39] for all O atomic orbitals.[40,41]

A detailed search was carried out to identify low-energy candidate anion structures. Initial structures were based on previously reported anions and neutrals.[10,15,42−44] The potential ground state geometries of anionic spin states (doublet and quartet) and neutral spin states (singlet and triplet) of $Zn_xO_x^{-/0}$ ($1 \leq x \leq 5$) clusters were calculated. Geometry optimizations were carried out using standard techniques, and optimized stationary points were characterized using analytic second-derivative calculations.[45]

For a direct comparison with the experimental results, neutral EA_0 values were computed as the difference between the zero-point energy (ZPE) corrected energies of the optimized neutral ground state and the anion ground state with the same structure. The EA_0 is an adiabatic detachment energy (ADE) associated with the transitions between the lowest energy state of a distinct structure of the anion to the lowest energy electronic state of the neutral with the same general structure. Additional ADEs were calculated to higher lying states of the neutral. EA_e values were also computed as the energy difference between the non-ZPE corrected energies of the optimized neutral and anion. Vertical detachment energies (VDEs), the energy at which the vibronic manifold reaches maximum intensity, generally are modeled as the difference in energy of the optimized anion (not ZPE-corrected) and the neutral confined to the structure of the anion. In cases where the neutral and anion structures are nearly identical, but the vibrational frequencies are very different, this approach can result in the VDE being lower in energy than the ADE, which is a nonphysical result, but can be interpreted as an indication that the origin transition is expected to be the most intense transition in the vibrational manifold. In the results presented below, EA_0, EA_e and VDE are close in energy, which is consistent with similar optimized anion and neutral structures.

Frank−Condon simulations were generated using home written LabView codes described in detail previously,[46] to further compare the computed results more thoroughly to the experimental results. The atomic positions, vibrational frequencies, and normal coordinates are given as the inputs for determining normal coordinate displacements. Using the EA_0 as the origin, the simulations were done incorporating combinations of up to 4 modes with temperature controlled independently for each mode. The vibrational bands can be convoluted with the experimental resolution, which is dependent on e^-KE (eq 3), though an input allows the resolutions to be scaled to either see stick spectra, or to approximate the effect of rotational broadening. Harmonic oscillator wave functions are used to approximate the vibrational wave functions of the anion and neutral in calculating the Franck−Condon factors. The code assumes the anion and neutral modes to be parallel, which is the appropriate approximation for the computed $Zn_xO_x^{-/0}$ structures, as their structures are similar.[11]

The Natural Ionization Orbital (NIO) model was employed to provide an orbital representation of the electron detachment in the $Zn_xO_x^-$ modeled by DFT calculations. Full details of the NIO model are available in the literature.[47] Briefly, the NIOs are given by a natural orbital transformation of the difference density, Δ_p,

$$\Delta_p = P^f - P^i \tag{5}$$

where P^i and P^f are defined as the initial state and final state density matrices, respectively. In the case of a single electron detachment, this analysis will yield one unpaired *detachment NIO* with an occupation change number of −1 electron and some number of *relaxation* NIO pairs with occupation change numbers that are equal in magnitude and opposite in sign. As discussed in detail in prior work, the detachment NIO is rigorously equivalent to the normalized Dyson orbital and the relaxation orbitals are interpreted as describing electronic relaxation in the final state in response to the electron loss.[47−49] Magnitudes of the occupation change numbers for the relaxation NIO pairs are related to the calculated pole strength;[50] the larger the magnitude of relaxation pair occupation change numbers, the smaller the pole strength. If an NIO analysis includes a relaxation pair with ±1 occupation change numbers, the transition corresponds to a two electron process (one detached electron and a one-electron excitation) and will yield a pole strength (and cross-section) of 0.

The Dyson orbital determined by the NIO analysis can be used to determine the PAD. In this work, we have employed a linear combination of atomic orbitals (LCAO) based approach to model the anisotropy parameter, β, according to eq 6

$$\beta = \sum |c_l^{\text{Dyson}}|^2 b_l \tag{6}$$

Where the atomic orbital expansion coefficients for the NIO Dyson orbital are grouped by their orbital angular momentum to give c_l^{Dyson}, values and b_l are parameters taken from Hanstorp's simplification of the Cooper-Zare equation.[51,52] Specifically, b_l values corresponding to l = 0,1,2,3 are 2.00, 0.00, 0.20, and 0.28. Despite its simplicity, this model provides qualitative results that align with conceptual expectations based on the nature and symmetry of the Dyson orbital given by the NIO model. Future work by one of our groups will examine the use and potential limitations of this model in detail; but such an analysis is beyond the scope of the current report. Using eqs 2 and 5 allows an important and additional point of corroboration between experiment and computation. The NIO based Dyson orbital has been used in this study to evaluate the pole strength, anisotropy parameter, and predicted spectral intensity at 0°, 90°, and integrated over all angles.

3. RESULTS AND DISCUSSION

Figure 1 shows a representative mass spectrum of $Zn_xO_y^-$ ions generated using the laser ablation source described above. A range of clusters in different overall oxidation states are produced, with each x having a different pattern in y. This mass spectrum is consistent with the mass spectrum published by Gunaratne et al. previously;[15] and based on our fits of the isotopologue manifolds, hyperoxide species ($y > x$) are intermingled with hydroxides. The insets show simulations of the natural isotopologue distribution with line widths of 0.4 units (solid trace) and convoluted to our experimental

https://doi.org/10.1021/acs.jpca.4c03613
J. Phys. Chem. A 2024, 128, 6450−6461

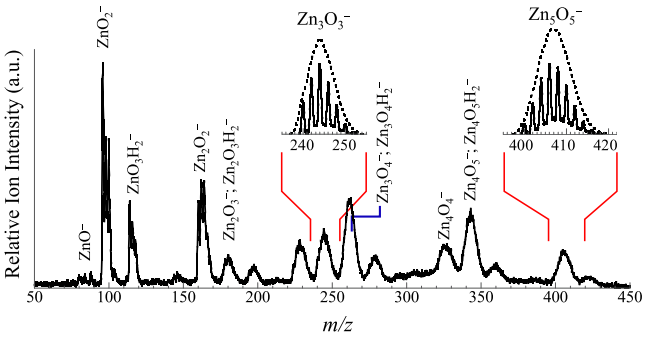

Figure 1. Mass spectrum of $Zn_xO_yH_z^-$ ions generated using the laser ablation source described in Section 2.2. Simulations of the isotopologue distributions of $Zn_3O_3^-$ and $Zn_5O_5^-$ are shown as insets. The solid lines show the distributions of isotopologues given a 0.3 m/z line width, and the dotted lines show the manifold convoluted to the experimental resolution. Note all hyperoxides except for ZnO_2^- can be fit assuming overlapping oxide and hydroxide distributions.

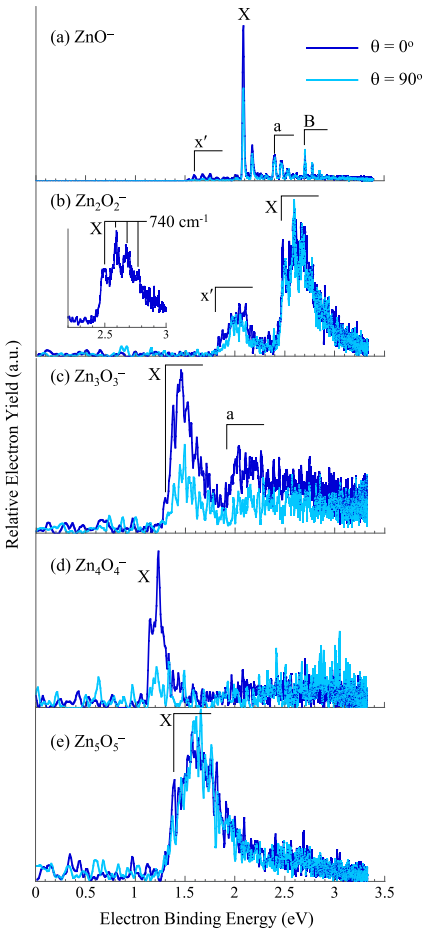

Figure 2. PE spectra of (a) ZnO^-, (b) $Zn_2O_2^-$, (c) $Zn_3O_3^-$, (d) $Zn_4O_4^-$, and (e) $Zn_5O_5^-$ obtained using 3.495 eV photon energy. Darker blue traces are spectra collected with the laser polarization parallel to the electron drift path, light blue traces with laser polarization perpendicular to the electron drift path. The PE spectrum of ZnO^- adapted from ref[22], Copyright 2001, with permission from Elsevier.

resolution (dotted trace), to illustrate the challenge in probing these species spectroscopically: The detachment laser overlaps with only one isotopologue based on the narrow appearance of the neutral signal observed during the experiments, so larger clusters are distributed over an increasingly broad range of m/z values. Note that if a more abundant isotopologe of the $Zn_xO_y^-$ cluster is being photodetachned, and if any $Zn_xO_yH_z^-$ is present, a less abundant isotopologue of the latter will coincide with the former.

We now present the anion PE spectra in detail.

3.1. PE Spectra. Figure 2 shows the PE spectrum of (a) ZnO^- from ref22 for direct comparison, and newly obtained PE spectra of (b) $Zn_2O_2^-$, (c) $Zn_3O_3^-$, (d) $Zn_4O_4^-$, and (e) $Zn_5O_5^-$, collected using 3.495 eV photon energy. Dark blue traces are spectra collected with the laser polarization parallel to the electron drift path, and light blue traces are the spectra collected with perpendicular polarization. Several features are labeled, and the associated detachment energies (EA_0 and VDE values) are summarized in Table 1. In contrast to the previously reported PE spectra of larger $Zn_xO_x^-$ ($x \geq 5$) clusters,[16] the binding energies do not change monotonically with x, though for x = 3, 4, and 5, the EA_0s are similar. However, there is a striking difference between the detachment transition energies of x = 2 and x = 3, which is more evocative of the punctuated evolution of properties in the small cluster size regime noted above.[3]

For x > 2, the most intense transitions are found at the lowest e^-BE, labeled X, and as will be rationalized below, band X in all five spectra are transitions from the ground state of the anion to the neutral ground state. Bands X are more intense in spectra collected with parallel polarization for ZnO^-, $Zn_3O_3^-$, and $Zn_4O_4^-$. Bands X are largely isotropic for $Zn_2O_2^-$ and $Zn_5O_5^-$. The PE spectrum of $Zn_5O_5^-$ is very similar to the spectrum reported by Heinzelmann et al.[16] New information from the spectrum presented here (Figure 2e) is the nearly isotropic photoelectron angular distribution.

While the spectra of all the polyatomic clusters show vibrational broadening, the only distinctive vibrational progression is observed for band X in the $Zn_2O_2^-$ spectrum. Band X is vibrationally congested, but exhibits a 740 cm^{-1} vibrational progression, in which each member of the progression is broadened, possibly by combination progressions in a lower frequency vibrational mode or modes (consistent with the computation-based simulation shown below), sequence bands, and broad rotational manifolds. The inset shows the sum of the spectra obtained at the two different polarizations, along with a comb set with a 740 cm^{-1} spacing. This value is close to the 720 cm^{-1} vibrational progression spacing exhibited in the PE spectrum of ZnO^- (band X) suggesting that the $Zn_2O_2^-$ molecular structure has at least one Zn═O terminal bond.

The spectrum of the ZnO^- diatomic anion was analyzed in detail previously, but a brief description of the electronic structure sets the stage for understanding the electronic structures of the larger species. The neutral ground state is a closed shell molecule with mixed ionic and covalent character. In simple terms, the Zn−O bond forms via the Zn 4s orbital and the O $2p_z$ orbital, with Zn described as Zn^{2+} ($3d^{10}$) and O as O^{2-} ($2p^6$), giving an overall $^1\Sigma^+$ electronic term. The excess electron in the neutral occupies a Zn 4s-like, marginally antibonding σ orbital. Therefore, the detachment transition is dominated by the origin transition, with a short vibrational progression, as can be seen in Figure 2a. Additional detachment transitions observed at higher e^-BE are associated

https://doi.org/10.1021/acs.jpca.4c03613
J. Phys. Chem. A 2024, 128, 6450−6461

Table 1. Experimental Peak Positions for the PE Spectra of $Zn_xO_x^-$ Shown in Figure 2, along with Computed Transition Energies[a]

cluster	band	EA_0/VDE (eV)	computed transition	comp. EA_0(eV)	comp. EA_e(eV)	comp. VDE(eV)
ZnO^-[b]	x′	1.67	($a^3\Pi \leftarrow a^2\Pi$)			
	X	**2.087**	($X^1\Sigma \leftarrow X^2\Sigma$)	2.31	2.31	2.36
	a	2.400	($a^3\Pi \leftarrow X^2\Sigma$)			
	B	2.706	($A^1\Pi \leftarrow X^2\Sigma$)			
$Zn_2O_2^-$	x′	1.90(5)/2.02(10)	$^1A_g \leftarrow {}^2A_g$ (rhombus)	2.12	2.10	2.14
	X	**2.48(2)**/2.59(5)	$^3A'' \leftarrow {}^2A'$ (bent chain)	2.49	2.48	2.53
$Zn_3O_3^-$	X	**1.34(4)**/1.45(3)	$^1A_1' \leftarrow {}^2A_1'$	1.58	1.54	1.62
	A	2.00(10)/-	*not assigned*			
$Zn_4O_4^-$	X	**1.145(5)**/1.23(1)	$^1A_{1g} \leftarrow {}^2A_{1g}$	1.39	1.33	1.39
$Zn_5O_5^-$	X	**1.376(10)**/1.59(2)	$^1A_1' \leftarrow {}^2A_1'$	1.50	1.45	1.57

[a]EA_0 represents the adiabatic electron affinity determined from the difference between the ZPE-corrected energies of the optimized neutral and anion state. EAe represents the EA determined from the difference between the non-ZPE corrected energies of the optimized neutral and anion. VDE is the difference in energy between the neutral confined to the structure of the anion, and the energy of the optimized anion (no ZPE corrections). [b]The values included for ZnO^- adapted from Reference 22. Copyright 2001, with permission from Elsevier.

with detachment of electrons from the nonbonding $\pi_{O\ 2p\perp}$ orbitals.

The PAD of the transition associated with detachment of the electron from the 4s-like singly occupied molecular orbital (SOMO) of the anion is parallel to the laser polarization, which is consistent from the Zn 4s parentage.[28,29] The PADs resulting from detachment associated with the $\pi_{O\ 2p\perp}$ orbitals are expected to be isotropic or perpendicular to the laser polarization, as they are seen to be in the experimental spectrum. The energy difference between these resulting $^3\Pi$ and $^1\Pi$ electronic states and the ground $^1\Sigma^+$ state gives the excitation energy of these states for direct spin-forbidden and spin-allowed absorption transitions. This excitation energy loosely correlates to the bulk band gap, or the energy required to promote an electron from the valence band (largely of O 2p parentage) and the conduction band (largely of Zn 4s and 4p parentage).[53] Clearly, the $\Pi-\Sigma$ transition energy in the diatomic is not comparable to the bulk ZnO band gap, 3.37 eV.

Without any preconceptions about the specific molecular structures, the electronic structures of the larger Zn_xO_x stoichiometric clusters are expected be described similarly, in that the constituent atoms in the neutrals can be described in terms of $3d^{10}$ Zn^{2+} and $2p^6$ O^{2-} ions. If the excess electron occupies a molecular orbital of Zn 4s parentage, we would further expect the transitions to be parallel. This is clearly the case for $Zn_3O_3^-$ and $Zn_4O_4^-$. In contrast, band X in both the PE spectra of $Zn_2O_2^-$ and $Zn_5O_5^-$ exhibit, on average, isotropic PAD. However, the low-e$^-$BE edges of the individual members of the 740 cm^{-1} progression of band X in the PE spectrum of $Zn_2O_2^-$, along with the low e$^-$BE edge of the partially resolved vibrational feature in the $Zn_5O_5^-$, are more intense in the spectra obtained with parallel polarization. These bands plotted on an expanded scale are included in the Supporting Information, for greater clarity. While vibronic coupling can result in variations in the photoelectron angular distribution over a vibrational manifold, what is observed here is an extreme example. We consider computational results on these species for more insight.

3.2. Lowest Energy Structures and Computed Relative Energies. A thorough range of possible cluster structures, including linear, planar, and three-dimensional structures, were attempted computationally. The results on the lowest energy computed structures are summarized in Figures 3 and 4.

Figure 3 shows schematics of the relative energies of the structural isomers computed for (a) $Zn_2O_2^-/Zn_2O_2$ and (b) $Zn_3O_3^-/Zn_3O_3$. Table 2 summarizes the computed energies of the anions and neutrals relative to the lowest energy structure of the anion, the electronic terms, and the EA_0 values for all $Zn_xO_x^-/Zn_xO_x$ ($2 \le x \le 5$). Previous computational studies predicted the rhombus (D_{2h}) structure to be the lowest energy for Zn_2O_2. However, the experimental PE spectrum suggests a structure with a terminal Zn═O bond. Indeed, in our computations, the lowest energy structure of the anion was predicted to have a bent O−Zn−O−Zn chain structure with C_s symmetry, shown in Figure 3a, with the D_{2h} structure of the anion computed to be 0.44 eV higher in energy. The corresponding neutral structures are calculated to be much closer in energy and as a result, the computed EA_0 of the chain structure is substantially higher than the D_{2h} structure. The ground electronic state of the bent chain neutral structure is a triplet state. Additional local minimum energy structures of $Zn_2O_2^-$ and Zn_2O_2 are included in Figure 3. The EA_0 values are indicated on the arrows connecting the anions to their respective neutral structures. The transition energies to excited spin states are included in Table 2.

The lowest energy structures of both anions and neutrals computed for Zn_xO_x (x = 3, 4, 5) are predicted to be high symmetry planar ring structures shown in Figures 3b and 4a,b. As with the D_{2h} structure of Zn_2O_2, the lowest lying neutral Zn_xO_x clusters are predicted to have a singlet ground state, and the anions are predicted to have a doublet ground state, as expected based on the heuristic picture of the electronic structures presented above. The quartet states were found to lie over 1 eV higher in energy than the doublet states. These ring structures are consistent with the structures computed previously by Wang et al.[13]

All the computed Zn_xO_x (x = 2, 3, 4, 5) ring structures shown in Figures 3 and 4, have D_{xh} symmetry, ignoring the negligible distortion that can be an artifact of the calculations (detailed structural information is included in the Supporting Information). Note that the energies of nonring structures become increasingly unfavorable with size in this narrow range of clusters. The bent chain structure of $Zn_3O_3^-$ shown in Figure 3b is relatively competitive with the D_{3h} ring, while for $Zn_4O_4^-$ and $Zn_5O_5^-$, the second lowest energy structures lie above the detachment continuum of the D_{xh} neutral structures. Taken together with the lowest energy chain structure for

https://doi.org/10.1021/acs.jpca.4c03613
J. Phys. Chem. A 2024, 128, 6450−6461

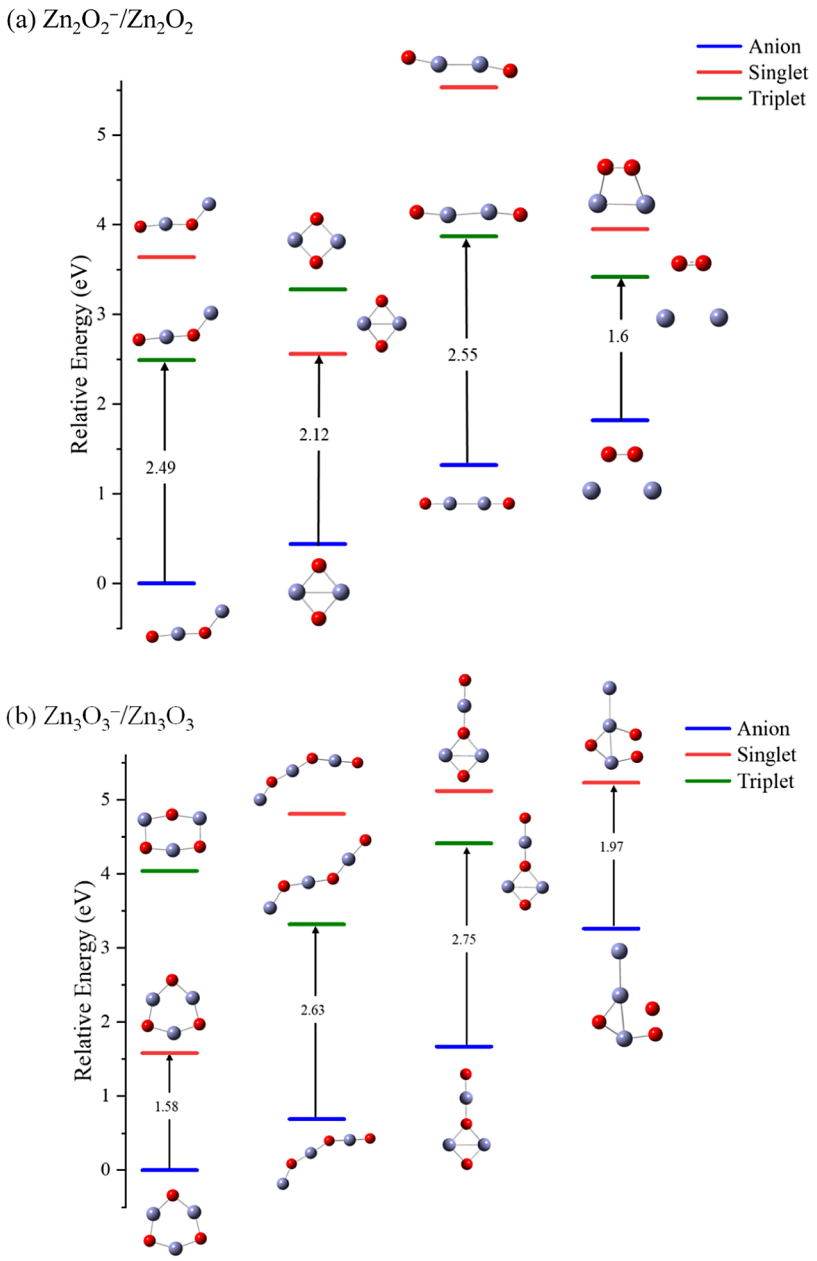

Figure 3. Lowest energy structural isomers determined for the (a) Zn_2O_2 and (b) Zn_3O_3 cluster anions and neutrals found computationally. The lowest energy bent chain structures of the anion and neutral were not identified in previous computational studies. Red represents the O atoms and slate blue represents the Zn atoms. Detailed structural parameters for the anions and neutrals are included in the Supporting Information.

$Zn_2O_2^-$, we conclude that ring strain trends from being unfavorable to unimportant between $x = 2$ and $x = 3$. In the size range considered in this study, 3-dimensional structures are not energetically competitive. Relative energies of all structures shown in Figures 3 and 4 are included in Table 2.

Based on the computational results, for the $Zn_3O_3^-$, $Zn_4O_4^-$ and $Zn_5O_5^-$ PE spectra, band X corresponds to the transition from the doublet anion state to the singlet neutral state of the ring structure. In the case of $Zn_2O_2^-$, band X corresponds to a transition from the doublet state of the anion to the triplet state of the neutral, which means the detachment transition is not associated with a Zn 4s-like SOMO, but rather the SOMO-1. The computed EA values, also summarized in Table 1, are all in reasonable agreement with the experimentally determined values, though they are systematically higher for $x > 2$, and slightly lower for $x = 2$. This can be readily reconciled with the known behavior of the hybrid functional used in this study, which is that higher spin states are overstabilized due to exchange.[54]

Further focusing on the $Zn_2O_2^-$ spectrum and the computational results, we can assert that band x′ is due to the presence of the higher-energy D_{2h} structure populating the molecular beam. As noted above, the relative intensity of band x′ changes with source conditions, which is the hallmark of a higher-energy structural isomer. The origin of band x′, 1.90 eV, is in reasonable agreement with the computed 2.12 eV EA_0 of the D_{2h} isomer. Therefore, we make the final assignment of band X to the transition from anion to the triplet neutral of the bent chain isomer, and band x′ to the transition from doublet anion to the singlet neutral of the ring structure. The

https://doi.org/10.1021/acs.jpca.4c03613
J. Phys. Chem. A 2024, 128, 6450−6461

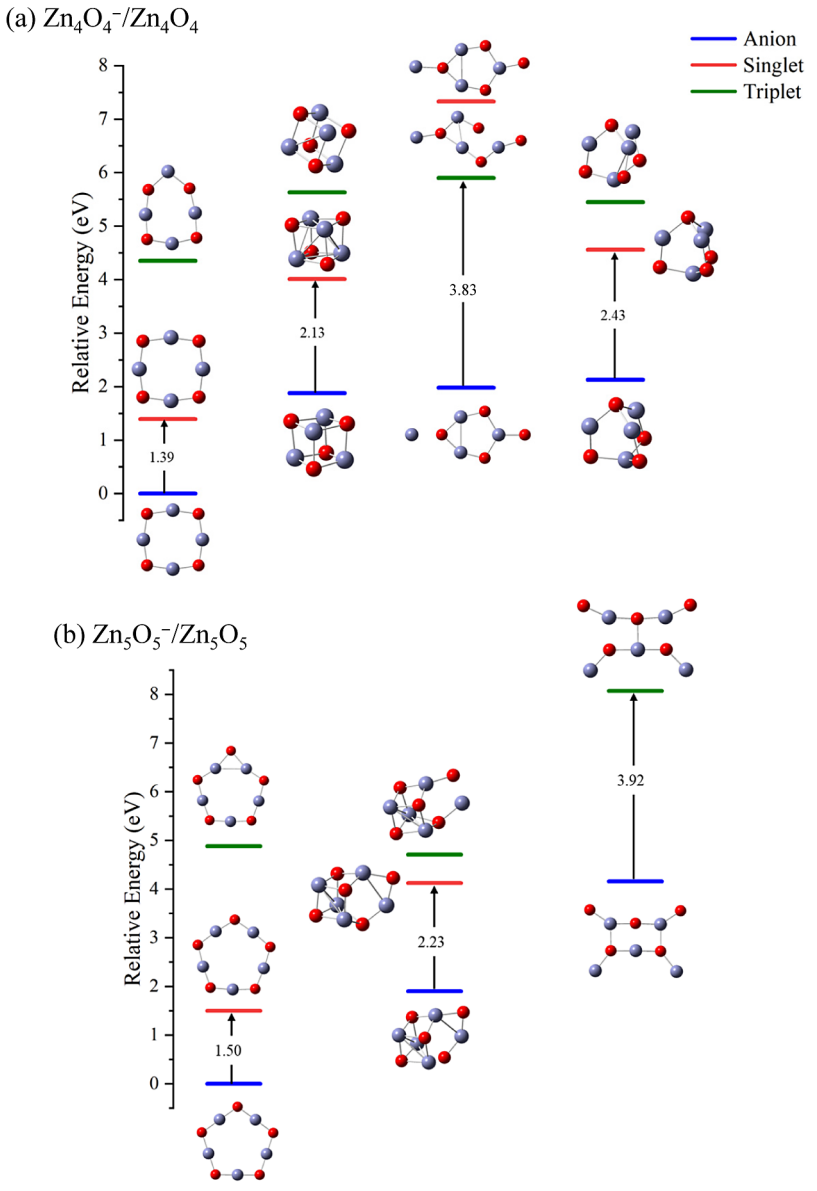

Figure 4. Lowest energy structural isomers determined for the (a) Zn_4O_4 and (b) Zn_5O_5 cluster anions and neutrals found computationally. The lowest energy bent chain structures of the anion and neutral were not identified in previous computational studies. Red represents the O atoms and slate blue represents the Zn atoms. Detailed structural parameters for the anions and neutrals are included in the Supporting Information.

calculations also predict a transition from anion ring structure to triplet state of the neutral at around 2.8 eV, which overlaps with the higher e$^-$BE portion of band X and would not be readily discerned.

3.3. Spectral Simulations and NIOs. A more quantitative comparison between the experimental and computational results can be achieved by generating simulations of the spectra based on the computed spectroscopic parameters. Figure 5 shows the simulated spectra generated from the computed EA_0 values, vibrational frequencies, and normal coordinates. The computed simulation parameters are summarized in Table 3, and depictions of the normal coordinates of the active modes are included in the Supporting Information.

The simulation for the bent chain structure of $Zn_2O_2^-$ is consistent with the extended progression in the Zn═O terminal bond stretch mode, though the computed frequency, 632 cm^{-1}, is lower than observed. As described below, the NIO is bonding with respect to the Zn═O terminal bond, and detachment results in a decrease in the vibrational frequency of the Zn═O stretch in the neutral relative to the anion, in addition to resulting in the extended progression.

In general, for the ring structures of Zn_2O_2, Zn_3O_3, and Zn_4O_4, the Zn−O−Zn bond angles are wider in the anion than neutral, but significantly smaller for Zn_5O_5 (108° for the anion, 115° for the neutral). The Zn−O bond lengths in the anions are approximately 0.020−0.025 Å longer than those for their associated neutrals. Compared to the bent chain structure of $Zn_2O_2^-$, the simulations for the ring structures have relatively short vibrational progressions, and in low-frequency totally symmetric ring distortion modes that monotonically decrease with increasing ring size from 279 cm^{-1} for Zn_2O_2 to 146 cm^{-1} for Zn_5O_5. These modes are indicated with asterisks in Table 3. The Zn−O stretch modes are less active, and also decrease monotonically with increasing ring size, from 637 cm^{-1} for

https://doi.org/10.1021/acs.jpca.4c03613
J. Phys. Chem. A 2024, 128, 6450−6461

Table 2. Summary of the Relative Energies (ZPE-Corrected) of the Lowest Lying States of the Lowest Energy Structures Computed for Zn_xO_x ($2 \leq x \leq 5$) Anions and Neutrals (Figures 3 and 4), Optimized at the B3LYP/SDDPlusTZ Level[a]

cluster	structure	term	relative E (eV)	ADE (eV)
Zn_2O_2	Zn−O−Zn−O (box)	$^3A'$	3.42	**1.60**/2.13
	O−Zn−Zn−O (linear chain)	$^3\Sigma_g^-$	3.87	**2.55**/4.21
	D_{2h} ring/rhombus	^1A_g	2.55	2.12/**2.84**
	Zn−O−Zn−O (bent chain)	$^3A''$	2.49	**2.49**/3.64
$Zn_2O_2^-$	Zn−O−O−Zn (box)	$^2B_2$	1.82	
	O−Zn−Zn−O (linear chain)	$^2\Sigma_g^+$	1.32	
	D_{2h} ring/rhombus	^2A_g	0.44	
	Zn−O−Zn−O (bent chain)	$^2A'$	0	
Zn_3O_3	C_s book	$^1A'$	5.23	1.97
	C_s tadpole/rhombus-plus chain	$^3A'$	4.42	**2.75**/3.45
	C_1 zigzag chain	^3A	3.32	**2.63**/4.12
	D_{3h} ring	$^1A_1'$	1.58	1.58/**4.04**
$Zn_3O_3^-$	C_s book	$^2A'$	3.26	
	C_s tadpole/rhombus-plus chain	$^2A'$	1.67	
	C_1 zigzag chain	^2A	0.69	
	D_{3h} ring	$^2A_1'$	0	
Zn_4O_4	cage	$^1A_1$	4.56	2.43/**3.32**
	tadpole	^3A	5.81	**3.83**/5.35
	T_d cube/rhombohedral	^1A	4.01	2.13/**4.10**
	D_{4h} ring	^1A	1.39	1.39/**4.35**
$Zn_4O_4^-$	cage	$^2A_1$	2.13	
	tadpole	^2A	1.98	
	T_d cube/rhombohedral	$^2A_1$	1.88	
	D_{4h} ring	$^2A_{1g}$	0	
Zn_5O_5	book	^3A	8.08	**3.92**
	dist. rhombohedron	^1A	4.12	2.23/**2.81**
	D_{5h} ring	$^1A_1'$	1.50	1.50/**4.88**
$Zn_5O_5^-$	book	$^2A'$	4.16	
	dist. rhombohedron	^2A	1.90	
	D_{5h} ring	$^2A_1'$	0	

[a]ADE values shown were determined from the difference in ZPE-corrected energies of the anions and neutrals with analogous structure. The ADEs associated with the triplet states are in bold face; by the ADE associate with the transition to the singlet states are in normal font. The lower-energy ADE is equivalent to the EA_0

Zn_2O_2 to 498 cm^{-1} for Zn_5O_5 (indicated with double asterisks in Table 3).

All simulated spectra of $Zn_xO_x^-$ ($x > 2$) have origins at 0.05 to 0.2 eV higher binding energy than the observed spectra, which, as noted above, is consistent with the computational method's systematic overstabilization of higher spin states relative to lower spin states.[54] We note here that there are no detachment transitions predicted for $Zn_3O_3^-$ that are consistent with band x′. The higher-energy chain structure of $Zn_3O_3^-$ shown in Figure 3b is predicted to have its detachment origin at 2.63 eV, which is over 0.6 eV higher than band x′ in the $Zn_3O_3^-$ spectrum. We therefore suggest that this feature at 2.1 eV could be due to trizincdioxohydroxide anion ($Zn_3O_3H^-$) which may be present in the ion beam.

Also shown in Figure 5 are the NIOs associated with each transition. For comparison, the NIOs and SOMOs for all cluster structures included in this study are included in Figure S6. In all cases except for the bent chain structure of $Zn_2O_2^-$, the NIO closely resembles the SOMO of the anion. Therefore, detachment of the D_{xh} anionic structures is consistent with the HF/Koopmans' Theorem framework. This conclusion is further supported by the near-unity pole strengths computed for the lowest energy structure $Zn_xO_x^-$ (x = 3, 4, 5) detachment transitions, summarized in Table 4. Pole strengths for all structures shown in Figures 3 and 4 are summarized in Table S3.

In the case of the bent chain structure of $Zn_2O_2^-$, the lowest energy transition is to the $^3A''$ state, and the π SOMO-1 of the anion involved in the detachment transition is more delocalized over the chain than the NIO (depictions of all bent chain Zn_2O_2 anion and neutral valence orbitals are included in the Supporting Information). The NIO and the SOMO-1 are qualitatively similar in appearance, but the relatively low pole strength, 0.6 (Table 4) indicates that the detachment transition is accompanied by electronic relaxation in the remnant neutral.

3.4. Experimental and Computed Photoelectron Angular Distributions. We now qualitatively consider the orbitals associated with the detachment transitions and the PADs, followed by a comparison with the computed results. The anisotropy parameters, β, determined experimentally using eq 3 for all the detachment transitions are summarized in Table 4. The nearly isotropic PAD in band X of the $Zn_2O_2^-$ PE spectrum ($\beta = 0.1$) is consistent with detachment of π orbitals of O 2p parentage, which would yield photoelectrons with s-wave and d-wave character. The d-wave contributions diminish

https://doi.org/10.1021/acs.jpca.4c03613
J. Phys. Chem. A 2024, 128, 6450−6461

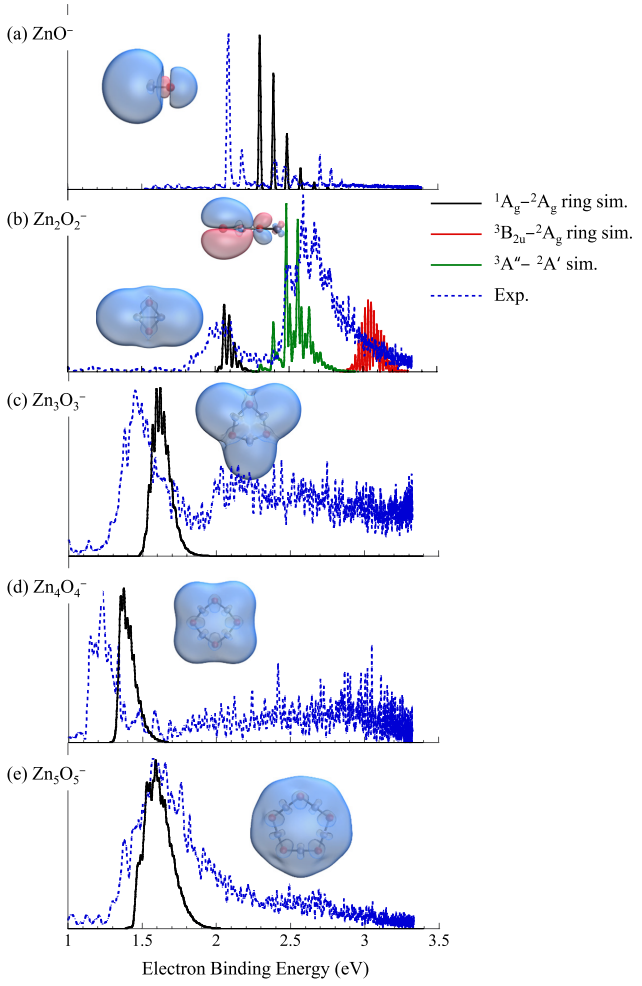

Figure 5. Spectral simulations of the anion PE spectra of (a) ZnO^-, (b) $Zn_2O_2^-$, (c) $Zn_3O_3^-$, (d) $Zn_4O_4^-$, and (e) $Zn_5O_5^-$ (solid traces) superimposed on the experimental spectra (dashed traces). Simulations are based on the computed zero-point corrected energies, molecular structures, vibrational modes and frequencies computed in this study. Table 3 summarizes the simulation parameters. In addition, the NIO computed for each detachment transition is included in each panel.

with lower e^-KE, so in this particular case, we anticipate the s-wave character to dominate, consistent with isotropic PAD.[28,29]

Considering the isosurfaces of the SOMO for the D_{xh} structures, which are totally symmetric in-phase combinations of the Zn 4s orbitals, we would anticipate parallel PADs.[28,29] Indeed, the experimental PADs for $Zn_3O_3^-$ (β = 0.7) and $Zn_4O_4^-$ (β = 0.9) determined from the relative intensities of the PE spectra obtained with parallel and perpendicular polarization and eq 3 are consistent with this qualitative picture. However, the $Zn_5O_5^-$ spectrum has nearly isotropic PAD, though this is not uniform across band X. The Supporting Information includes the spectra obtained with laser polarization parallel and perpendicular to the electron drift direction on expanded scales to highlight how the asymmetry varies over the breadth of the vibrational manifolds. In the $Zn_5O_5^-$ PE spectrum in particular, the origin is more intense in the parallel spectrum (β = 0.5), while near the most intense portion of band X, the perpendicular spectrum is modestly more intense, for an overall β = 0.

Table 4 includes the asymmetry parameters (β) computed using the NIOs. The calculations correctly predict an isotropic $^3A'' - {}^2A'$ detachment transition for the bent chain structure of $Zn_2O_2^-$. Distinctly parallel transitions are predicted for all anions with D_{xh} structures, as expected based on the symmetry of the SOMO, so there is clear disagreement in the case of $Zn_5O_5^-$. Since these highly symmetric structures have degenerate vibrational modes that when populated result in a vibronic state with $l > 0$, though it is not clear why the same effect is not observed over all the D_{xh} symmetry clusters. The observed variation in β across the vibronic manifold does suggest vibronic coupling. We will be investigating this disagreement between theory and experiment further, including exploring the possibility of vibronic coupling between the doublet ground state of the anion and low-lying degenerate doublet states, e.g., those accessed by promoting the lone electron from the a_1' SOMO to the degenerate e_1' orbital, also composed of Zn 4s orbitals. With increasing ring size, the energy difference between the 4s-based SOMO and LUMO would be expected to decrease, which increases the strength of vibronic coupling between these states.

3.5. Computed Singlet–Triplet Splitting in the D_{xh} Ring Structures. While this study is anchored in the experimentally measured PE spectra and calculations on the lowest energy electronic states for each structure, the calculations can provide insights that fall outside of our experimental capabilities. For example, in small stoichiometric (i.e., closed-shell) clusters, the singlet–triplet splitting correlates to the bulk band gap. For zinc oxide bulk band gap is 3.37 eV. Except for the bent chain Zn_2O_2 structure (as well as the ZnO diatomic), all the ring structures have singlet ground states, but the photon energies available in the laboratory to not allow us to measure the energies of the transitions to the triplet states.

For the nanoparticles in the quantum size effect regime, the band gap is larger than the bulk limit, but smoothly approaches the bulk limit as the size is increased.[5−8] For the small stoichiometric clusters studied in this work, in which the molecular structures in no way resemble the bulk 3-dimensional structure, the calculated singlet–triplet splitting is at or *below* the bulk band gap, suggesting that these small ring structures have very stable LUMOs. The singlet–triplet splitting increases with increase in the size of the ring structure from x = 2 to 5, as depicted in Figure 6. This is consistent with the calculations done by Zaragoza et al.[9] As noted above, the photon energy used in our experiment is not sufficient to access the triplet states of the ring structures, but the calculations, which are validated by their agreement with the transitions we are able to observe experimentally, do provide this additional insight, and could inform the development of small ring-based functionalized ZnO clusters for potential future applications.

4. CONCLUSIONS

New anion PE spectra of $Zn_xO_x^-$ (x = 2–5) were presented and interpreted with supporting DFT calculations. The PE spectra of the $Zn_xO_x^-$ (x = 3–5) clusters were consistent with spectral simulations generated from spectroscopic parameters computed for high-symmetry planar ring structures with D_{xh} symmetry, all of which were computed to be the lowest energy structures. In contrast, the PE spectrum of $Zn_2O_2^-$ appeared to have contributions to two structural isomers. The most intense spectroscopic feature showed a vibrational progression

https://doi.org/10.1021/acs.jpca.4c03613
J. Phys. Chem. A 2024, 128, 6450–6461

Table 3. Parameters from the Computed Relative Energies of the Anions and Neutrals, their Structures, Vibrational Frequencies and Normal Coordinates, Used in Generating the PE Spectral Simulations Shown in Figure 5[a]

cluster	transition (band)	origin (eV)	neutral frequency (cm^{-1})	anion frequency (cm^{-1})	mass weighted displacement (Å $amu^{1/2}$)
ZnO^-	$X^1\Sigma \leftarrow X^2\Sigma$ (X)	2.30	741	610	0.27
$Zn_2O_2^-$	$^1A_g \leftarrow {}^2A_g$ (x′;ring)	2.06	279*	256	0.48
			637**	599	0.11
	$^3B_{3g} \leftarrow {}^2A_g$ (ring)	2.83	203*	256	1.8
			560**	599	0.25
	$^3A'' \leftarrow {}^2A'$ (X bent)	2.48	820	625	0.006
			632	701	0.28
			418	392	0.12
			64	69	0.162
$Zn_3O_3^-$	$^1A_1' \leftarrow {}^2A_1'$ (X)	1.54	146	72	0.04
			147	72	0.006
			210*	193	0.91
			580**	534	0.126
$Zn_4O_4^-$	$^1A_{1g} \leftarrow {}^2A_{1g}$ (X)	1.35	171*	139	0.68
			540**	483	0.23
$Zn_5O_5^-$	$^1A_1' \leftarrow {}^2A_1'$ (X)	1.475	146*	95	1.04
			498**	471	0.466

[a]A vibrational temperature of 300 K was assumed for all modes in the simulations. Totally symmetric ring distortion modes are indicated by asterisks (*) and totally symmetric ring Zn−O stretch modes are indicated with double asterisks (**)

Table 4. Computed Pole Strengths and Corresponding Asymmetry Parameters (β) for $Zn_xO_x^-$($2 \le x \le 5$) Photodetachment Transitions[a]

structure	pole strength	β (computed)	β (expt)
C_s Zn_2O_2 bent chain ($^3A'' - {}^2A'$)	0.60	0.0	0.1
D_{2h} $Zn_2O_2^-$ rhombus	0.978	1.4	0.2
D_{3h} $Zn_3O_3^-$ ring	0.987	1.7	0.7
D_{4h} $Zn_4O_4^-$ ring	0.989	1.7	1.0
D_{5h} $Zn_5O_5^-$ ring	0.984	1.4	0.0

[a]All transitions involve the anion doublet to neutral singlet transition, with the exception of the $Zn_2O_2^-$ bent chain, for which the lowest energy detachment transition involves the neutral triplet state.

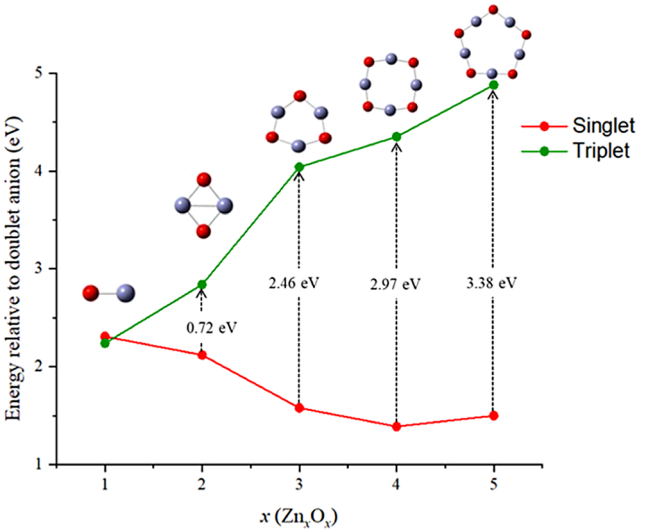

Figure 6. Singlet−triplet splittings computed for the D_{xh} structures of Zn_xO_x for x = 2−5 in addition to the computed splitting for ZnO diatomic. Note that for ZnO, the singlet state is the ground state of the neutral; the triplet state lies 0.313 eV higher in energy. This level of error associated with the systematic overstabilization of higher spin states relative to lower spin states is typical of the computational method used.

consistent with a Zn═O terminal bond, and was therefore not consistent with a D_{2h} ring structure previously predicted by others[10−12] to be the lowest energy structure. In calculations reported here, a bent chain structure of $Zn_2O_2^-$ emerged as being lower in energy than the ring structure. Calculations additionally provided insights into the singlet−triplet splitting in the ring structures, which in stoichiometric clusters, correlates to the bulk band gap. Our studies show that the ring structures have singlet−triplet splittings lower than the bulk band gap but increase monotonically with ring size from x = 2 to x = 5.

The PADs measured for the $Zn_xO_x^-$ (x = 2, 3, and 4) spectra were consistent with the orbitals associated with the detachment transitions, and are in qualitative agreement with the computed asymmetry parameters. However, the PAD measured for the $Zn_5O_5^-$ spectrum is puzzling and has inspired further theoretical investigation into why the detachment yields a nearly isotropic distribution, rather than the expected parallel distribution.

Finally, we highlight the observation that, while the small cluster size regime is typically characterized by punctuated changes in properties with incremental changes in size, for these Zn_xO_x anions and neutrals, the evolution of properties is gradual along the series of clusters with D_{xh} ring structures, the increasing size of which does not change the qualitative description of the electronic structure of the clusters.

■ ASSOCIATED CONTENT

Supporting Information

The Supporting Information is available free of charge at https://pubs.acs.org/doi/10.1021/acs.jpca.4c03613.

PE spectra of all anions shown on expanded scales to highlight the variation in β across the vibrational manifolds of the detachment transitions, sums of the spectra obtained with different polarization angles, detailed structural parameters for all anions and neutrals,

https://doi.org/10.1021/acs.jpca.4c03613
J. Phys. Chem. A 2024, 128, 6450−6461

valence orbitals for the bent chain of Zn_2O_2 doublet anion and triplet neutral, energies of quartet states of anions relative to doublets, pole strengths computed for all structures of all anions, $\langle S^2 \rangle$ values for the anions and neutrals, NIO/Dyson orbitals along with α HOMO (SOMO) for all anions, normal coordinates for vibrational modes active in the spectral simulations, and the Cartesian coordinates for the optimized geometries of the doublet anions (PDF)

AUTHOR INFORMATION

Corresponding Author

Caroline Chick Jarrold − *Department of Chemistry, Indiana University, Bloomington, Indiana 47405, United States;* orcid.org/0000-0001-9725-4581; Email: cjarrold@indiana.edu

Authors

Shivangi Vaish − *Department of Chemistry, Indiana University, Bloomington, Indiana 47405, United States*

Abigail O. Gyamfi − *Department of Chemistry and Biochemistry, University of California, Merced, California 95343, United States;* orcid.org/0000-0002-5545-7820

Caleb D. Huizenga − *Department of Chemistry, Indiana University, Bloomington, Indiana 47405, United States*

Hrant P. Hratchian − *Department of Chemistry and Biochemistry, University of California, Merced, California 95343, United States;* orcid.org/0000-0003-1436-5257

Complete contact information is available at: https://pubs.acs.org/10.1021/acs.jpca.4c03613

Notes

The authors declare no competing financial interest.

ACKNOWLEDGMENTS

This work was supported by the Department of Energy Grant DE-SC0024282 and National Science Foundation grants CHE-1848580 and OAC-2019144. We thank Ms. Abbey McMahon for her contributions to preliminary data collection and calculations.

REFERENCES

(1) Jena, P.; Castleman, A. W. Nanoclusters A bridge across Disciplines. In *Science and Techmology of Atomic, Molecular, Condensed Matter & Biological Systems* Jena, P.; Castleman, A. W., Eds.; Elsevier: Oxford, 2010; pp. 136.

(2) Kaldor, A. P.; Cox, D. M.; Zakin, M. R. Molecular Surfaces: Chemistry and Physics of Gas Phase Clusters. In *Microclusters*, Springer Series in Materials Sciences, Sugano, S.; Nishina, Y.; Ohnishi, S., Eds.; Springer: Berlin, Heidelberg, 1987; Vol. *4*.

(3) Mason, J. L.; Folluo, C. N.; Jarrold, C. C. More than Little Fragments of Matter: Electronic and Molecular Structures of Clusters. *J. Chem. Phys.* **2021**, *154* (20), 200901.

(4) Kumar, K. S.; Prajapati, G. L.; Dagar, R.; Vagadia, M.; Rana, D. S.; Tonouchi, M. Terahertz Electrodynamics in Transition Metal Oxides. *Adv. Opt. Mater.* **2020**, *8* (3), 1900958.

(5) Rao, C. N. R. Transition Metal Oxides. *Annu. Rev. Phys. Chem.* **1989**, *40*, 291−326.

(6) Pearton, S. J.; Norton, D. P.; Heo, Y. W.; Tien, L. C.; Ivill, M. P.; Li, Y.; Kang, B. S.; Ren, F.; Kelly, J.; Hebard, A. F. ZnO Spintronics and Nanowire Devices. *J. Elec. Magt* **2006**, *35*, 862−868.

(7) Kim, Y. H.; Kim, J. S.; Kim, W. M.; Seong, T.-Y.; Lee, J.; Muller-Meskamp, L.; Leo, K. Realizing the potential of ZnO with alternative non-metallic co-dopants as electrode materials for small molecule optoelectronic devices. *Adv. Funct. Mater.* **2013**, *23* (29), 3645−3652.

(8) Lange, I.; Reiter, S.; Patzel, M.; Zykov, A.; Nefedov, A.; Hildebrandt, J.; Hecht, S.; Kowarik, S.; Wol, C.; Heimel, G.; Neher, D. Tuning the Work Function of Polar Zinc Oxide Surfaces using Modified Phosphonic Acid Self-Assembled Monolayers. *Adv. Funct. Mater.* **2014**, *24* (44), 7014−7024.

(9) Zaragoza, I.-P.; Soriano-Agueda, L.-A.; Hernandez-Esparza, R.; Vargas, R.; Garza, J. Analyzing ZnO clusters through the density-functional theory. *J. Mol. Model.* **2018**, *24* (7), 164.

(10) Wang, B.; Nagase, S.; Zhao, J.; Wang, G. Structural Growth Sequences and Electronic Properties of Zinc Oxide Clusters $(ZnO)_n$ (n = 2−28). *J. Phys. Chem. C* **2007**, *111* (111), 4956−5963.

(11) Wang, X.; Wang, B.; Tang, L.; Sai, L.; Zhao, J. What is Atomic Structures of $(ZnO)_{34}$ Magic Cluster? *Phys. Lett. A* **2010**, *374*, 850−853.

(12) Zhao, M.; Xia, Y.; Tan, Z.; Liu, X.; Mei, L. Design and Energetic Characterization of ZnO Clusters from First Principles Calculations. *Phys. Lett. A* **2007**, *372*, 39−43.

(13) Wang, B.; Wang, X.; Zhao, J. Atomic Structure of the Magic $(ZnO)_{60}$ Cluster: First Principles Predictoin of a Sodalite Motif for ZnO Nanoclusters. *J. Phys. Chem. C* **2010**, *114*, 5741−5744.

(14) Barcaro, G.; Monti, S.; Sementa, L.; Carravetta, V. *J. Chem. Theory Comput.* **2019**, *15*, 2010−2021.

(15) Gunaratne, K. D. D.; Berkdemir, C.; Harmon, C. L.; Castleman Jr, A. W. Investigating the Relative Stabilities and Electronic Properties of Small Zinc Oxide Clusters. *J. Phys. Chem. A* **2012**, *116*, 12429−12437.

(16) Heinzelmann, J.; Koop, A.; Proch, S.; Gantefor, G. F.; Lazarski, R.; Sierka, M. Cage-Like Nanoclusters of ZnO Probed by Time-Resolved Photoelectron Spectroscopy and Theory. *J. Phys. Chem. Lett.* **2014**, *5*, 2642−2648.

(17) Mann, J. E.; Mayhall, N. J.; Jarrold, C. C. Properties of Metal Oxide Clusters in Non-Traditional Oxidation States. *Chem. Phys. Lett.* **2012**, *525*−*526*, 1−12.

(18) Mann, J. E.; Waller, S. E.; Rothgeb, D. W.; Jarrold, C. C. Study of Nb2O y (y = 2−5) anion and neutral clusters using anion photoelectron spectroscopy and density functional theory calculations. *J. Chem. Phys.* **2011**, *135* (10), 104317.

(19) Rothgeb, D. W.; Mann, J. E.; Jarrold, C. C. H_2 Production from Reactions Between Water and Small Molybdenum Suboxide Cluster Anions. *J. Chem. Phys.* **2010**, *133* (5), 054305.

(20) Ray, M.; Waller, S. E.; Saha, A.; Raghavachari, K.; Jarrold, C. C. Comparative Study of Water Reactivity with $Mo_2O_y^-$ and $W_2O_y^-$ Clusters: A Combined Experimental and Theoretical Investigation. *J. Chem. Phys.* **2014**, *141* (10), 104310.

(21) Rodriguez, J. A.; Grinter, D. C.; Liu, Z.; Palomino, R. M.; Senanayake, S. D. Ceria-Based Model Catalysts: Fundamental Studies on the Importance of the Metal-Ceria Interface in CO Oxidation, the Water-Gas Shift, CO_2 Hydrogenation, and Methane and Alcohol Reforming. *Chem. Soc. Rev.* **2017**, *46*, 1824−1841.

(22) Moravec, V. D.; Klopcic, S. A.; Chatterjee, B.; Jarrold, C. C. The Electronic Structure of ZnO and ZnF Determined by Anion Photoelectron Spectroscopy. *Chem. Phys. Lett.* **2001**, *341*, 313−318.

(23) Harrison, J. F.; Field, R. W.; Jarrold, C. C. Comparison of CaF, ZnF, CaO, and ZnO: Their Anions and Cations in their Ground and Low-Lying States. In *Low-Lying Potential Energy Surfaces*, Hoffmann, M. R.; Dyall, K. G., Eds.; ACS, 2002; Vol. *828*.

(24) Kim, J. H.; Li, X.; Wang, L.-S.; DeClercq, H. L.; Fancher, C. A.; Thomas, O. C.; Bowen, K. H. Vibrationally Resolved Photoelectron Spectroscopy of MgO^- an ZnO^- and the Low-Lying Electronic States of MgO, MgO^- and ZnO. *J. Chem. Phys. A* **2001**, *105*, 5709−5718.

(25) Moravec, V. D.; Jarrold, C. C. Study of the Low-Lying States of NiO^- and NiO Using Anion Photoelectron Spectroscopy. *J. Chem. Phys.* **1998**, *108*, 1804−1810.

(26) Waller, S. E.; Mann, J. E.; Jarrold, C. C. Asymmetric Partitioning of Metals among Cluster Anions and Cations Generated via Laser Ablation of Mixed Aluminum/Group 6 Transition Metal Targets. *J. Phys. Chem. A* **2013**, *117*, 1765−1772.

(27) Felton, J. A.; Ray, M.; Jarrold, C. C. Measurement of the Electron Affinity of Atomic Ce. *Phys. Rev. A* **2014**, *89*, 033407.
(28) Cooper, J.; Zare, R. N. Angular Distribution of Photoelectrons. *J. Chem. Phys.* **1968**, *48*, 942−943.
(29) Sanov, A. Laboratory-Frame Photoelectron Angular Distributions in Anion Photodetachment: Insight into Electronic Structure and Intermolecular Interactions. *Annu. Rev. Phys. Chem.* **2014**, *65*, 341−363.
(30) Frisch, M. J.; Trucks, G. W.; Schlegel, H. B.; Scuseria, G. E.; Robb, M. A.; Cheeseman, J. R.; Scalmani, G.; Barone, V.; Petersson, G. A.; Nakatsuji, et al. *Gaussian Development Version Revision I.09*; Gaussian Inc.: Wallingford CT, 2016.
(31) Frisch, M. J.; Trucks, G. W.; Schlegel, H. B.; Scuseria, G. E.; Robb, M. A.; Cheeseman, J. R.; Scalmani, G.; Barone, V.; Mennucci, B.; Petersson, G. A., et al. *GAUSSIAN 16*; Gaussian Inc: Wallingford, CT, USA, 2016.
(32) Becke, A. D. Density-Functional Thermochemistry. III. The Role of Exact Exchange. *J. Chem. Phys.* **1993**, *98*, 5648−5652.
(33) Lee, C.; Yang, W.; Parr, R. G. Development of the Colle-Salvetti Correlation-Energy Formula into a Functional of the Electron Density. *Phys. Rev. B* **1988**, *37*, 785−789.
(34) Mason, J. L.; Harb, H.; Abou Taka, A.; Huizenga, C. D.; Corzo, H. H.; Hratchian, H. P.; Jarrold, C. C. New Photoelecron-Valence Electron Interactions Evident in the Photoelectron Spectrum of Gd_2O^-. *J. Phys. Chem. A* **2021**, *125*, 9892−9903.
(35) Mason, J. L.; Harb, H.; Abou Taka, A.; McMahon, A. J.; Huizenga, C. D.; Corzo, H.; Hratchian, H. P.; Jarrold, C. C. Photoelectron Spectra of Gd 2 O 2 − and Nonmonotonic Photon-Energy-Dependent Variations in Populations of Close-Lying Neutral States. *J. Phys. Chem. A* **2021**, *125* (3), 857−866.
(36) Mason, J. L.; Harb, H.; Huizenga, C. D.; Ewigleben, J. C.; Topolski, J. E.; Hratchian, H. P.; Jarrold, C. C. Electronic and Molecular Structures of the CeB_6 Monomer. *J. Phys. Chem. A* **2019**, *123*, 2040−2048.
(37) Mason, J. L.; Harb, H.; Topolski, J. E.; Hratchian, H. P.; Jarrold, C. C. A Tale of Two Stabilities: How One Boron Atom Affects a Switch in Bonding Motifs in $CeO_2B_x^-$ (x = 2, 3, Complexes. *J. Phys. Chem. A* **2018**, *122*, 9879−9885.
(38) Topolski, J. E.; Kafader, J. O.; Marrero-Colon, V.; Iyengar, S. S.; Hratchian, H. P.; Jarrold, C. C. Exotic electronic structures of SmxCe3−xOy (x = 0-3; y = 2-4) clusters and the effect of high neutral density of low-lying states on photodetachment transition intensities. *J. Chem. Phys.* **2018**, *149* (5), 054305.
(39) Dunning, T. H., Jr. Gaussian Basis sets for use in Correlated Molecular Calculations. I. the Atoms Boron through Neon and Hydrogen. *J. Chem. Phys.* **1989**, *90*, 1007−1023.
(40) Waller, S. E.; Mann, J. E.; Rothgeb, D. W.; Jarrold, C. C. Study of $MoNbO_y$ (y = 2 - 5) Anion and Neutral Clusters using Photoelectron Spectroscopy and Density Functional Theory Calculations: Impact of Spin Contamination on Single Point Calculations. *J. Phys. Chem. A* **2012**, *116*, 9639−9652.
(41) Mayhall, N. J.; Rothgeb, D. W.; Hossain, E.; Raghavachari, K.; Jarrold, C. C. Electronic Structures of $MoWO_y^-$ and $MoWO_y$ Determined by Anion Photoelectron Spectroscopy and DFT Calculations. *J. Chem. Phys.* **2009**, *130* (12), 124313.
(42) Jain, A.; Kumar, V.; Kawazoe, Y. Ring Structures of Small ZnO Clusters. *Comput. Mater. Sci.* **2006**, *36*, 258−262.
(43) Chen, M.; Straatsma, T. P.; Fang, Z.; Dixon, D. A. Structural and Electronic Property Study of $(ZnO)_n$, $n \leq 168$: Transition from Zinc Oxide Molecular Clusters to Ultrasmall Nanoparticles. *J. Phys. Chem. C* **2016**, *120*, 20400−20418.
(44) Sharma, M.; Mishra, D. DFT+U Study of Small ZnO Nanoclusters. *AIP Conf. Proc.* **2019**, *2142*, 110025.
(45) Hratchian, H. P.; Schlegel, H. B. Finding Minima Transition States, and Following Reaction Pathways on Ab Initio Potential Energy Surfaces. In *Theory and Applications of Computational Chemistry: the First 40 Years*, Dykstra, C. E.; Kim, K. S.; Frenking, G.; Scuseria, G. E., Eds.; Elsevier, 2005; pp. 195249. DOI: DOI: 10.1016/B978-044451719-7/50053-6.
(46) Schaugaard, R. N.; Topolski, J. E.; Ray, M.; Raghavachari, K.; Jarrold, C. C. Insight into Ethylene Interactions with Molybdenum Suboxide Cluster Anions from Photoelectron Spectra of Chemifragments. *J. Chem. Phys.* **2018**, *148* (5), 054308.
(47) Thompson, L. M.; Harb, H.; Hratchian, H. P. Natural Ionization Orbitals for Interpreting Electron Detachment Processes. *J. Chem. Phys.* **2016**, *144* (20), 204117.
(48) Harb, H.; Hratchian, H. P. ΔSCF Dyson Orbitals and Pole Strengths from Natural Ionization Orbitals. *J. Chem. Phys.* **2021**, *154* (8), 084104.
(49) Ortiz, J. V. Dyson-Orbital Concepts for Description of Electrons in Molecules. *J. Chem. Phys.* **2020**, *153* (7), 070902.
(50) Ortiz, J. V. Electron Propagator Theory: An Approach to Prediction and Interpretation in Quantum Chemistry. *WIREs Comput. Mol. Sci.* **2013**, *3* (2), 123−142.
(51) Hanstorp, D.; Bengtsson, C.; Larson, D. J. Angular Distributions in Photodetachment from O^-. *Phys. Rev. A* **1989**, *40*, 670−675.
(52) Grumbling, E.; Sanov, A. Photoelectron angular distributions in negative-ion photodetachment from mixed sp states. *J. Chem. Phys.* **2011**, *135* (16), 164302.
(53) Wu, H.-C.; Peng, Y.-C.; Shen, T.-P. Electronic and Optical Properties of Substitutional and Interstitial Si-Doped ZnO. *Materials* **2012**, *5*, 2088−2100.
(54) Harvey, J. N. DFT Computation of Relative Spin-State Energetics of Transition Metal Compounds. In *Principles and Applications of Density Functional Theory in Inorganic Chemistry I*, Structure and Bonding, Kaltsoyannis, N.; McGrady, J. E., Eds.; Springer: Berlin, Heidelberg, 2004; pp. 151184. DOI: DOI: 10.1007/b97939.

https://doi.org/10.1021/acs.jpca.4c03613
J. Phys. Chem. A 2024, 128, 6450−6461